ChemBioChem

Research Article
doi.org/10.1002/cbic.202300579

Chemistry Europe
European Chemical Societies Publishing

www.chembiochem.org

VIP *Very Important Paper*

Inducin Triggers LC3-Lipidation and ESCRT-Mediated Lysosomal Membrane Repair

Dale Corkery[+],[a] Andrei Ursu[+],[b] Belén Lucas[+],[b] Michael Grigalunas[+],[b] Simon Kriegler,[c] Rosario Oliva,[c, e] Robert Dec,[c] Sandra Koska,[b] Axel Pahl,[b] Sonja Sievers,[b] Slava Ziegler,[b] Roland Winter,[c] Yao-Wen Wu,[a] and Herbert Waldmann*[b, d]

Lipidation of the LC3 protein has frequently been employed as a marker of autophagy. However, LC3-lipidation is also triggered by stimuli not related to canonical autophagy. Therefore, characterization of the driving parameters for LC3 lipidation is crucial to understanding the biological roles of LC3. We identified a pseudo-natural product, termed Inducin, that increases LC3 lipidation independently of canonical autophagy, impairs lysosomal function and rapidly recruits Galectin 3 to lysosomes. Inducin treatment promotes Endosomal Sorting Complex Required for Transport (ESCRT)-dependent membrane repair and transcription factor EB (TFEB)-dependent lysosome biogenesis ultimately leading to cell death.

Introduction

Autophagy is an evolutionarily conserved degradation program that eliminates damaged proteins, protein aggregates and damaged organelles to sustain proper cell function and homeostasis.[1] Autophagy can be induced by stress conditions like nutrient deprivation or viral infections and proceeds through the generation of double membranes that engulf cytoplasmic components into vesicles termed autophagosomes. Degradation of the enclosed material occurs upon fusion of autophagosomes with lysosomes. A hallmark of autophagy is the covalent attachment of the ubiquitin-like protein LC3 to the lipid phosphatidylethanolamine (to yield LC3-II) by the E3-like ATG conjugation complex (ATG12-ATG5-ATG16L1) on nascent autophagosomal membranes. Consequently, LC3-II has historically been used as a marker of autophagosomes. However, LC3 lipidation has been shown to also play a key role in several cellular processes beyond autophagic degradation pathways that require autophagosome formation.[2] These "non-canonical" pathways often result in LC3 conjugation to single-membrane compartments and occur independent of part of the core autophagy machinery. These scenarios emphasize the importance of proper experimental design for correct data interpretation of altered LC3 lipidation levels in cells.[3] Importantly, the unconventional LC3 lipidation onto damaged lysosomal membranes has been shown to be independent of the autophagy machinery upstream of the ATG conjugation system. This parallel LC3-dependent pathway regulates calcium efflux essential for the induction of TFEB-dependent lysosome biogenesis.[4] Lysosomal membrane damage, also referred to as lysosomal membrane permeabilization (LMP), can be triggered by different stimuli like bacteria and small molecules and is implicated in the pathogenesis of several neurodegenerative diseases.[5] The lysosomal fate strongly depends on the extent of LMP, and lysosomal membrane rupture can either be repaired by the endosomal sorting complex required for transport (ESCRT) machinery or damaged lysosomes can be removed by a selective macroautophagic pathway (lysophagy).[6] However, severe and extensive LMP eventually leads to lysosome-dependent cell death, which is cathepsin-dependent and may proceed as necrosis.[7]

Small molecules are invaluable tools for the dissection of biological processes. While many different physiological stimuli have been shown to compromise lysosomal integrity, our understanding of the cellular response to LMP is derived primarily from studies that employ the dipeptide L-leucyl-L-leucine O-methyl ester (LLOMe). LLOMe enters the lysosome via receptor-mediated endocytosis and undergoes Cathepin C-

[a] Dr. D. Corkery,[+] Prof. Dr. Y.-W. Wu
Department of Chemistry
Umeå University
Umeå Centre for Microbial Research
Umeå SE-90187 (Sweden)

[b] Dr. A. Ursu,[+] Dr. B. Lucas,[+] Dr. M. Grigalunas,[+] S. Koska, Dr. A. Pahl, Dr. S. Sievers, Dr. S. Ziegler, Prof. Dr. Dr. H. Waldmann
Department of Chemical Biology
Max Planck Institute of Molecular Physiology
Otto-Hahn-Strasse 11, 44227 Dortmund (Germany)

[c] S. Kriegler, Dr. R. Oliva, Dr. R. Dec, Prof. Dr. R. Winter
Physical Chemistry I – Biophysical Chemistry
Department of Chemistry and Chemical Biology
TU Dortmund University
Otto-Hahn-Strasse 4a, 44227 Dortmund, Germany

[d] Prof. Dr. Dr. H. Waldmann
Faculty of Chemistry and Chemical Biology
Technical University Dortmund
Otto-Hahn-Strasse 6, Dortmund 44227 (Germany)

[e] Dr. R. Oliva
Present address: Department of Chemical Sciences
University of Naples Federico II
Via Cintia 4, Naples 80126 (Italy)

[+] These authors contributed equally to this manuscript.

Supporting information for this article is available on the WWW under https://doi.org/10.1002/cbic.202300579

dependent polymerization to form a membranolytic polymer.[8] The discovery of small molecules that trigger LMP through alternative mechanisms may broaden our understanding of the endomembrane damage response and is, therefore, valuable for LMP-related research. Here, we report a compound class based on the natural product Sinomenine that induces unconventional LC3 lipidation in cells independently of canonical autophagy. The most potent derivative, termed Inducin, is a lysosomotropic compound that induces LMP, ESCRT-mediated lysosomal repair and, eventually, cell death.

Results and Discussion

In the course of a program aimed at the development of bioactive pseudo-natural products (PNPs),[9] we designed a Sinomenine-indole (SM–I) PNP class in which the fragment-sized natural product (NP) Sinomenine was combined with indole fragments. Sinomenine is a morphan-containing NP and shares structural similarities to well-known opiates, such as morphine; however, Sinomenine's stereocenters have opposite configurations relative to morphine, resulting in different bioactivities. According to the PNP principle, the combination of NP-fragments or fragment-sized NPs in novel arrangements not found in nature may yield novel NP-like compound classes with unexpected bioactivity.[9c,10] Therefore, the combination of Sinomenine and indole fragments promised to yield new bioactive chemical matter.

We have previously employed this design principle for the synthesis of a small Sinomenine-derived compound collection.[10a] Here, we describe the expansion of this SM–I collection and an investigation of its biological activities. The synthesis of the SM–I collection was initiated with commercially available Sinomenine (**1**, Figure 1A). Via a hydrogenation and acid-mediated ring forming-elimination reaction sequence, ketone **2a** could be obtained in 69% yield over two steps (Figure 1A). Reductive zinc-mediated ring opening of **2a** afforded ketone **2b** in a high yield (94%). Ketones **2a** and **2b** were suitable substrates for Fischer indole reactions in which various phenylhydrazines were reacted under acid-catalyzed conditions to install indole fragments in a single complexity-generating step to effectively construct the scaffold of the SM–Is (**3** and **4**, respectively). Further SM–I derivatives were accessible through manipulation of the Sinomenine moiety (**5a**–**5d**, Figure S1). In total, 53 SM–Is were synthesized.

The biological activity of the compound collection was investigated in several phenotypic assays monitoring Hedgehog signaling, autophagy and kynurenine production. Several PNPs increased LC3 puncta formation after amino-acid starvation of MCF7 cells that stably express EGFP-LC3 (see Figure 1B and Table S1–S3). In addition, an increase in LC3 puncta was observed when autophagy was induced by the mTOR inhibitor Rapamycin (Figure 1B and Table S1–S3). Dimethylated compound **3t** was the most potent derivative in both assays and at a concentration of 10 μM increased the number of LC3 puncta by 271 ± 80% and 607 ± 195% for amino-acid starvation and Rapamycin treatment respectively (Figure 1C). Derivatives with the same indole substitution pattern as **3t** also led to a significant increase in LC3 puncta (**3u**, **3v**, and **3y**) whereas the deletion of one (**3b** and **3o**) or both (**3a**) methyl substituents on the indole phenyl ring led to an almost complete loss in activity. Retaining the indole methylation pattern of **3t** and derivatizing the Sinomenine *N*-Me or *O*-Me moieties also led to a loss in activity (**5b** and **5d**, respectively). Therefore, specific indole substitution patterns without any modifications of the Sinomenine moiety appear to be necessary for activity in the assay (Figure 1C, Tables S1–S3). In a manual setup, the most potent compound **3t** at 5 μM triggered an approximately 14.5- and 4.5-fold increase in the number of EGFP-LC3 puncta per cell upon amino acid starvation or Rapamycin co-treatment (Figure 2A and 2B) which is comparable to the influence of the lysosomotropic compound Chloroquine (50 μM) and the V-ATPase inhibitor Bafilomycin A (0.1 μM, Figure 2A and 2B). Interestingly, **3t** increased the number of EGFP-LC3 puncta also in the absence of any autophagy induction (i.e., in plain medium, Figure 2C) and induced LC3 lipidation (Figure 2D) and, therefore, compound **3t** was termed Inducin. Under starvation conditions, Sinomenine did not alter the number of EGFP-LC3 puncta (Figure 2A), indicating that the biological activity of Inducin is reliant on fusing Sinomenine with an indole fragment (Figure 1B).

While the covalent attachment of LC3 to phosphatidylethanolamine on nascent autophagosomal membranes remains a hallmark of macroautophagy, LC3 lipidation can also occur in response to the activation of several non-autophagic pathways.[11] To characterize the mechanism underlying LC3 lipidation following Inducin treatment, we first examined LC3 lipidation in mouse embryonic fibroblasts (MEFs) deficient of the ULK1-interacting protein FIP200. FIP200 is essential for autophagosome initiation in macroautophagy,[12] but dispensable for most other non-autophagic pathways utilizing lipidated LC3.[3–4,13] Dose-dependent LC3 lipidation was observed in Inducin-treated FIP200 −/− MEFs (Figure 3A) indicating activation of a non-canonical autophagy pathway. LC3 lipidation was, however, completely abolished in ATG5 −/− MEFs (Figure 3A), confirming utilization of the downstream ubiquitin-like conjugation system.

Immunostaining of Inducin-treated wild-type (WT) MEFs revealed that compound treatment leads to the accumulation of LC3 and the autophagic cargo adaptor protein p62/SQSTM1 on vesicular structures within the cytosol (Figure 3B). One cellular process which utilizes both canonical and non-canonical LC3 lipidation is the response to endolysosomal membrane damage.[4,14] To determine if the LC3/p62 enriched vesicular structures observed upon Inducin treatment correspond to damaged endolysosomal membranes, we used Galectin-3 (Gal3) as a marker of damage.[15] Gal3 is a cytosolic carbohydrate-binding protein with affinity for β-galactosides. As most β-galactose-containing glycoconjugates are present on the exterior surface of the plasma membrane, endosomal lumen, or lysosomal glycocalyx, this interaction is spatially restricted. Extensive damage to any of these membranes will expose the β-galactosides to the cytosol and rapidly recruit Gal3, which acts as a signaling platform for subsequent membrane repair

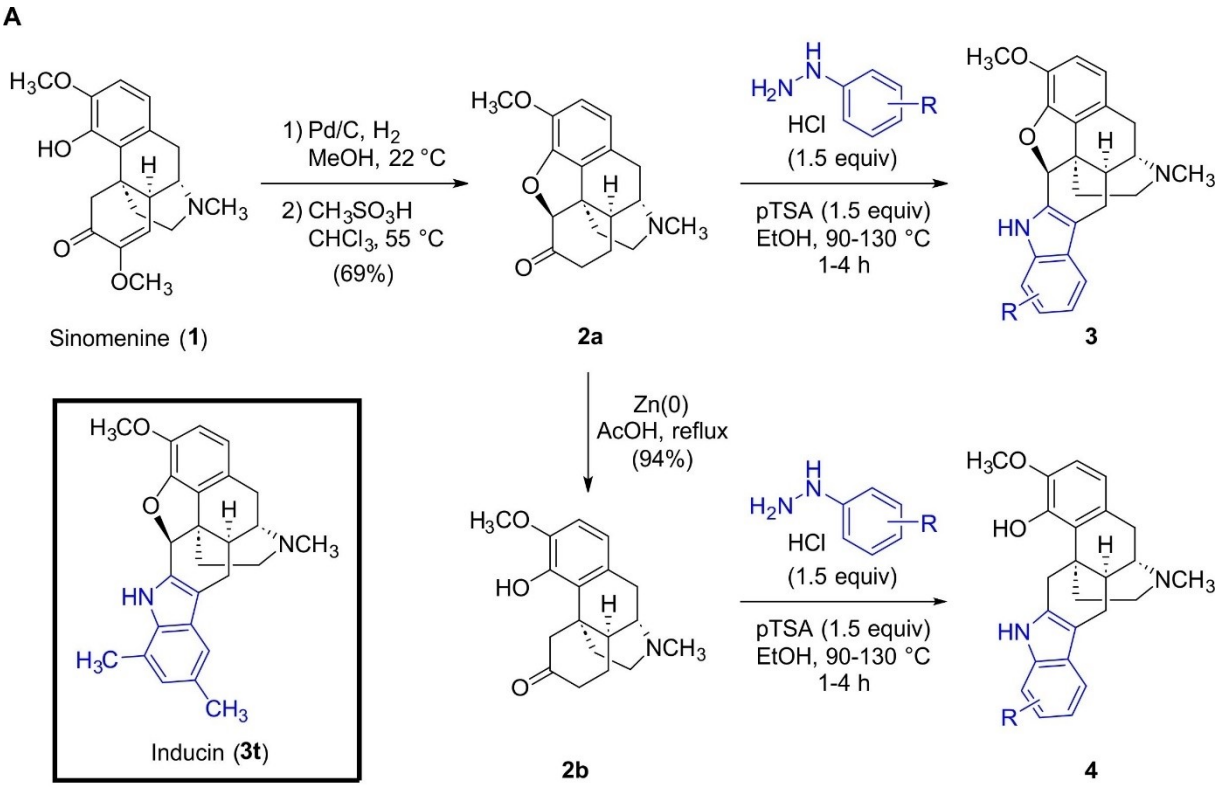

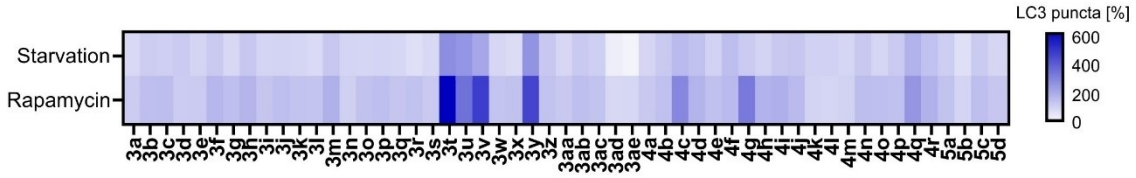

C

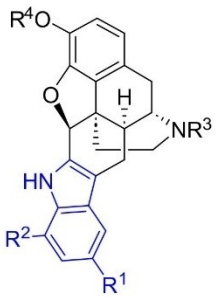

Cpd	R¹	R²	R³	R⁴	LC3 puncta (Starvation) [%]	LC3 puncta (Rapamycin) [%]
3a	H	H	Me	Me	90 ± 6	121 ±11
3b	Me	H	Me	Me	118 ± 6	151 ± 15
3o	H	Me	Me	Me	99 ± 5	145 ± 14
3t	Me	Me	Me	Me	271 ± 80	607 ± 195
3u	OMe	Me	Me	Me	250 ± 52	337 ± 103
3v	Cl	Me	Me	Me	210 ± 92	463 ± 342
3y	Me	Cl	Me	Me	256 ± 70	445 ±251
5b	Me	Me	Ac	Me	75 ± 6	101 ± 3
5d	Me	Me	Me	Allyl	97 ± 9	135 ± 8

Figure 1. Synthesis and biological activity of the Sinomenine-based PNP collection. (A) Synthesis of a Sinomenine-indole collection (**3**-**5**) starting from the natural product Sinomenine (**1**). (B) LC3 puncta detection in MCF7-EGFP-LC3 cells upon stimulation of autophagy by means of amino acid starvation (= starvation) or mTOR inhibition using Rapamycin. Compound concentration: 10 μM. The number of LC3 puncta was set to 100% for cells that were exposed to amino acid starvation or Rapamycin, respectively. Data are mean values of n = 3. See also Table S1–S3. (C) Structure-activity relationship for selected Sinomenine-indoles in the assays monitoring LC3 puncta in MCF7-EGFP-LC3 cells upon stimulation of autophagy by means of amino acid starvation (= starvation) or mTOR inhibition using Rapamycin. Compound concentration: 10 μM. The number of LC3 puncta was set to 100% for cells that were exposed to amino acid starvation or Rapamycin, respectively. Data are mean values (n ≥ 3) ± SD. See also Figure S1 and Tables S1–S4.

and removal pathways.[16] Using HeLa or MEF cells transiently transfected with EGFP-Gal3 and the lysosomal marker LAMP1-mCherry, we observed rapid recruitment of Gal3 to lysosomes within 5 min of Inducin treatment (Figure 3C and 3D). Co-

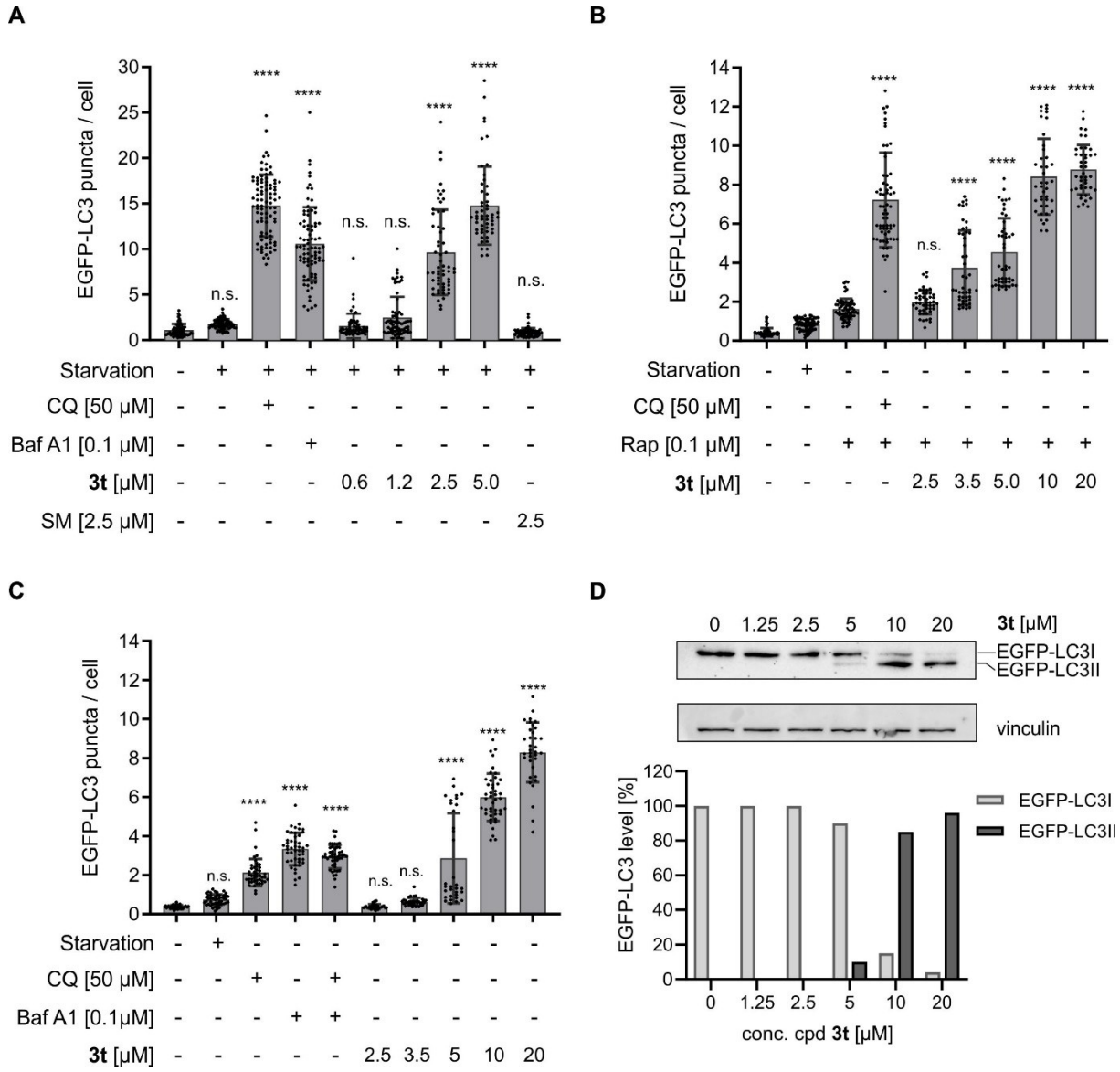

Figure 2. Influence of derivative **3t** on LC3 puncta formation. EGFP-LC3 puncta formation was monitored upon amino acid starvation (A), Rapamycin treatment (B) or without any stimulus (C) in the presence of different compound concentrations in MCF7-EGFP-LC3 after treatment for 3 h. (Data are mean values (n = 3) ± SD. Baf A1: Bafilomycin A1; CQ: Chloroquine; Rap: Rapamycin. SM: Sinomenine. Significance in comparison to starvation (A), Rapamycin treatment (B) or non-treated condition (C) was determined from biological replicates using an ordinary one-way ANOVA test. ****$p < 0.0001$. (D) Detection of EGFP-LC3I and EGFP-LC3II upon treatment of MCF7-EGFP-LC3 for 3 h using immunoblotting. Vinculin was detected as a loading control. The graph shows the quantification of band intensities. Data are representative of n = 3.

staining of Inducin-treated, EGFP-Gal3 transfected HeLa cells for endogenous LC3 and LAMP1 confirmed LC3 enrichment at damaged lysosomes (Figure 3E).

The cellular response to lysosomal damage involves three integrated pathways: (1) ESCRT-mediated repair of damaged membranes, (2) Autophagy-mediated clearance of unrepairable membranes (Lysophagy), and (3) Transcription factor EB (TFEB)-mediated replacement of lysosomes.[16] To further confirm lysosomal membrane damage as a result of Inducin treatment, we examined ESCRT machinery localization before and after treatment. ALIX, a component of the ESCRT machinery implicated in lysosomal membrane repair,[6a,17] was recruited to lysosomes in response to treatment with either the lysosomal-membrane-damaging agent L-leucyl-L-leucine O-methyl ester (LLOMe)[8] or 20 µM Inducin (Figure S2). This data confirms activation of the ESCRT-mediated lysosomal membrane repair pathway in response to Inducin treatment.

The third branch of the cellular response to lysosomal membrane damage involves the TFEB-mediated induction of lysosome biogenesis. TFEB translocates from the cytosol to the nucleus in response to lysosomal membrane damage[18] in a process dependent on non-canonical (FIP200-independent) LC3 lipidation.[4] Using HeLa cells stably expressing mNeonGreen-TFEB, we examined the subcellular localization of TFEB in response to Inducin treatment. Treatment with LLOMe or Inducin (20 µM) caused a significant TFEB nuclear translocation

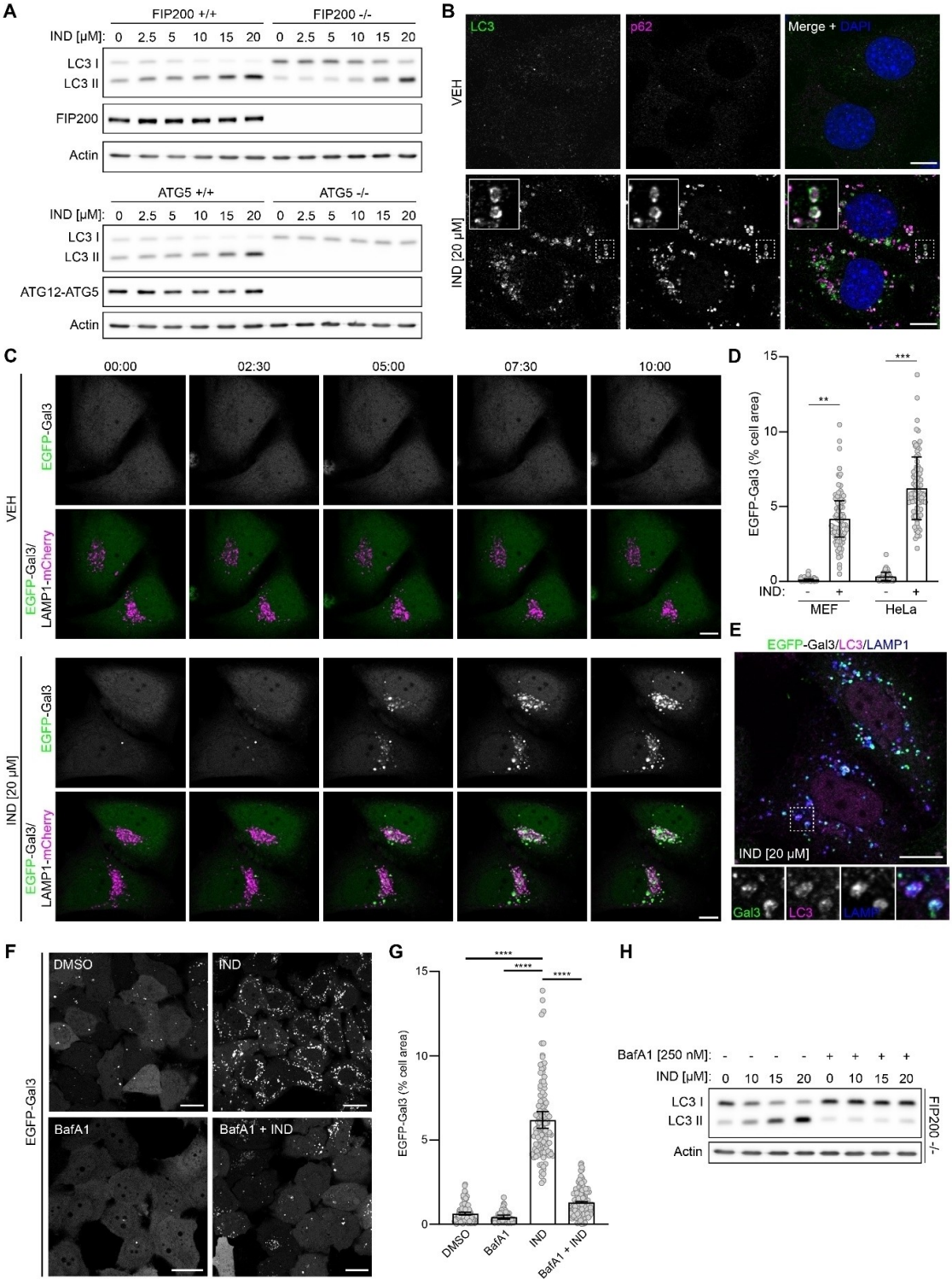

Figure 3. Inducin triggers LC3 lipidation at damaged lysosomal membranes. (A) Western blot analysis of WT and FIP200-deficient or ATG5-deficient MEFs treated with the indicated concentrations of Inducin for 2 h. (B) WT MEFs treated with DMSO or 20 μM Inducin for 2 h and co-stained for LC3 and p62. Nuclei were counterstained with DAPI. Scale bars: 10 μm. (C) Live-cell imaging of HeLa cells transiently transfected with EGFP-Gal3/LAMP1-mCherry and treated with vehicle or 20 μM Inducin for the indicated time points. Scale bar: 10 μm. (D) Quantification of the percentage of cell area occupied by EGFP-Gal3 puncta in MEF and HeLa cells transiently transfected with EGFP-Gal3 and treated with vehicle or 20 μM Inducin for 30 min. Bars show mean ± SD (n = 3). Data points represent individual cells pooled from the three independent experiments (n > 25 cells per experiment). Significance was determined from biological replicates using a two-tailed, unpaired t-test. **p = 0.0045, ***p = 0.0001. (E) HeLa cells transiently transfected with EGFP-Gal3, treated with 20 μM Inducin for 2 h and co-stained for endogenous LC3 and LAMP1. Scale bar: 10 μm. (F–H) Inducin activity is V-ATPase dependent. (F) HeLa cells transiently transfected with EGFP-Gal3 and treated with the indicated compounds for 20 min. Inducin: 20 μM, BafA1: 250 nM. Scale bars: 20 μm. (G) Quantification of EGFP-Galectin 3 puncta from (F) Bars show mean ± SD (n = 3). Data points represent individual cells pooled from the three independent experiments (n = 40 cells per experiment). Significance was determined from biological replicates using an ordinary one-way ANOVA with Tukey's multiple comparisons test. ****p < 0.0001. (H) Western blot analysis of FIP200-deficient MEFs treated as indicated for 30 min. Baf A1: Bafilomycin A1. See also Figure S2 and S3.

(Figure S3A–S3C). TFEB activation was further confirmed by Western blot as its activation is regulated via dephosphorylation,[19] which is detected as a down-shift in molecular weight (Figure S3D).

Together, these data show that the LC3 lipidation observed after Inducin treatment is a consequence of lysosomal membrane damage. The activity of V-ATPase, which acidifies lysosomes, is linked to non-canonical LC3 lipidation via direct recruitment of ATG16L1 to target membranes[20] and is important for LC3 lipidation by the lysosomotropic agent Chloroquine.[21] Therefore, we analysed the influence of Bafilomycin A1[22] on the lysosomal damage caused by Inducin. Indeed, co-treatment of cells with Baf A1 and Inducin prevented both the recruitment of Gal 3 to lysosomes (Figure 3F and 3G) and LC3 lipidation (Figure 3H), indicating that the activity of Inducin depends on V-ATPase and lysosomal acidification.

Lysosomal damage can be caused by accumulation of weakly basic, lipophilic compounds in lysosomes. This lysosomotropism leads to protonation and trapping of basic, lipophilic compounds in the acidic milieu of the lysosomes.[23] As a result, lysosomal pH rises, which impairs the function of various lysosomal enzymes. Lysosomotropic compounds share similar physicochemical properties of logP >2 and pKa between 6.5 and 11,[24] and this also applies to all compounds of the Sinomenine-based PNP library besides **5b** (Figure 4A and Table S4). The LysoTracker DND-99 dye itself gets enriched in lysosomes at low pH. Pretreatment of U2OS cells with Inducin concentration-dependently prevented staining of lysosomes using LysoTracker DND-99 (Figure 4B).

The structurally similar derivative **3a**, which lacks both methyl groups on the indole phenyl ring but features an identical bpKa value with Inducin, is much less active with regard to LC3 puncta formation, and reduced lysosomal staining only at high concentrations (Figure 4B). The relatively less basic N-acetylated derivative **5b** did not influence the LysoTracker staining (Figure 4B), which is in line with its physicochemical properties of pKa $=-0.99$ and logP $=3.81$ (Figure 4A). These findings suggest that Inducin and, to a lesser extent, **3a** may accumulate in lysosomes which is in agreement with their physicochemical properties.

Lysosomal compound accumulation has been linked to impaired cholesterol transport out of lysosomes.[23] Accordingly, treatment with Inducin but not compounds **3a** and **5b** led to accumulation of cholesterol inside vesicular structures, most likely lysosomes (Figure 4C). Lysosomotropic compounds impair the activity of lysosomal enzymes, for example lipases, which is linked to the formation of multilamellar bodies that are the cause of lipid excess, known as phospholipidosis.[25] Phospholipidosis can be detected microscopically using HCS LipidTOX™ Red phospholipidosis detection reagent. Indeed, increased lipid content was detected in the presence of 2.5 μM Inducin (Figure 4D). Lysosomal damage can eventually cause cell death. Treatment of HeLa or U2OS cells with Inducin reduced cell growth and increased cell death at 5 and 10 μM, but not at 2.5 μM or lower concentrations as detected by activation of caspase-3/7 and propidium iodide (PI) staining (Figure 4E and 4F and Figure S4). Compound **5b** did not influence cell growth, while compound **3a** caused cell death at 10 μM (Figure S5).

Overall, our findings reveal that Inducin impairs lysosomal function. At low concentration (i.e., 2.5 μM) phospholipidosis, but no durable lysosomal damage is observed, whereas at higher concentrations (≥ 5 μM) Inducin damages lysosomes and, eventually, causes cell death. Interestingly, the time-resolved cell death analysis revealed activation of caspase-3/7 within 4 to 8 h upon addition of Inducin in parallel to loss of membrane integrity as detected by PI staining. These results are in line with LMP as the probable cause of cell death. Lysosomal damage leads to release of lysosomal proteases like cathepsin D that may activate caspase-3/7, whereas, in parallel, plasma membrane integrity is lost either due to detergent-like properties of the lysosomotropic compound or in a lysosomal protease-dependent manner.[26]

Seemingly, Inducin exhibits a rather unique behavior among the Sinomenine-based PNP collection. Its lysosomotropic properties may account for the observed effects, however, most derivatives of the explored compound collection classify as lysosomotropic agents according to their physicochemical properties (see Figure 4A), but they do not increase LC3 puncta formation at 10 μM. Therefore, Inducin exhibits a unique mode of action that goes beyond classic lysosomotropism.

In order to elucidate whether Inducin modulates the properties of lipid bilayers, model lysosomal membranes represented by overall negatively charged liposomes composed of POPC and POPG (85/15 mol/mol) were treated with Inducin, compounds **3a** and **5b** or Siramesine as a control for lysosomotropism. Changes in fluidity, lipid order and hydration level were determined by means of fluorescence spectroscopy at 25 °C and pH 7.4 and pH 5.0 using two widely used membrane fluorescent probes, Laurdan and 1,6-diphenyl-1,3,5-hexatriene (DPH).[27] Only small changes in the general polarization *(GP)*-values and DPH anisotropy were observed in presence of the compounds at both pHs, indicating that they do not alter the packing in the head group region of the bilayer significantly and high fluidity is preserved in the bilayer hydrophobic core (Figure S6). To examine if stable partitioning of the compounds in the lipid bilayer is in fact low, we recorded temperature-dependent fluorescence spectra on the corresponding phospholipid system having saturated C16-chains, i.e., DPPC/DPPG (85/15 mol/mol), which exhibits a gel-to-fluid lipid phase transition at $T_m = 42$ °C at neutral pH. No marked changes in DPH anisotropy values and hence lipid packing and dynamics were observed in the presence of the compounds (Figure S7). In a second set of experiments, we employed a membrane system mimicking more closely the composition of the lysosomal membrane[28] and prepared a negatively charged lysosomal model membrane using six major components, i.e., PC/Chol/SM/PE/BmP/PI at a molar ratio of 30/30/15/11/7/7 (for details of liposome preparation and composition see the Methods section and Figure S8). Compound addition did not cause any significant changes in the *GP*-value of Laurdan (Figure S9A), indicating that the compounds do not significantly modify the packing and lipid order of the model biomembrane. At pH 5.0 and 7.4, minor changes were detected at high

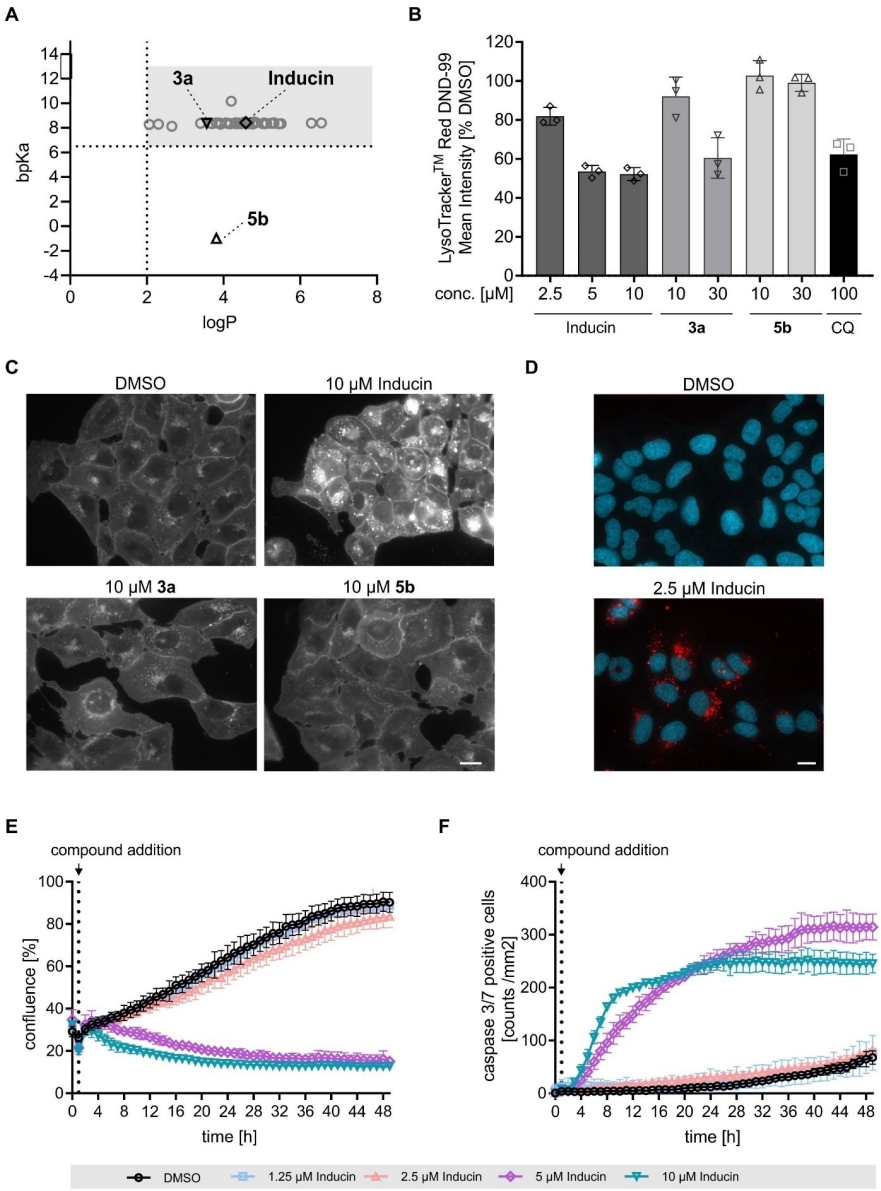

Figure 4. Inducin impairs lysosomes. (**A**) Calculated logP and bpKa values for the Sinomenine-based PNP collection. The gray region corresponds to properties of lysosomotropic compounds (logP > 2 and bpKa between 6.5 and 11). (B) Staining of lysosomes. U2OS cells were treated for 1 h with the compounds prior to fixation and staining using LysoTracker Red DND-99 and Hoechst 33342. Data are mean values (n = 3) ± SD. CQ: Chloroquine. (C) Cholesterol distribution in U2OS cells. Cells were treated with the compounds for 3 h prior to staining of cholesterol using Filipin. Scale bar: 20 µm. Representative images of three independent experiments (n = 3). (D) Phospholipidosis detection. U2OS cells were treated with DMSO or Inducin and HCS LipidTOX™ Red reagent (red) for 48 h. Cells were stained with Hoechst-33342 (blue) for nuclei detection. Scale bar: 20 µm. Representative images for n = 3. (E–F) Influence of Inducin on cell growth and cell death. HeLa cells were treated with Inducin or DMSO as a control in presence of the caspase 3/7 reagent. Cell growth (E) and caspase-3/7 activity (F) were monitored by means of live-cell analysis using IncuCyte Zoom. Data are representative of three independent experiments. See also Figure S4 and S5.

compound concentrations only (Figure S9B), indicating that also in these more elaborate membrane models the packing of lipid chains is not affected (Figure S9C and S9D).

To reveal topological changes of the lipid vesicles and their stability against leakage upon treatment with Inducin, confocal fluorescence microscopy using giant unilamellar vesicles (GUVs) were performed at pH 5 and 7. The GUVs composed of POPC and POPG are topologically stable over hours and have sizes in the micrometer range (5-10 µm). Upon addition of 6 µM Inducin, some leakage was observed already after 30 min (Figure 5). Complete loss of the encapsulated fluorophore was observed after 45 min. Remarkably, no changes in the morphology of the vesicles were detected. For compounds **3a** and **5b**, no leakage was observed even after 2 h of incubation (Figure S10), which is in line with their lower activity in cells. These results indicate that Inducin causes leakage without significantly altering the integrity of the lipid bilayer.

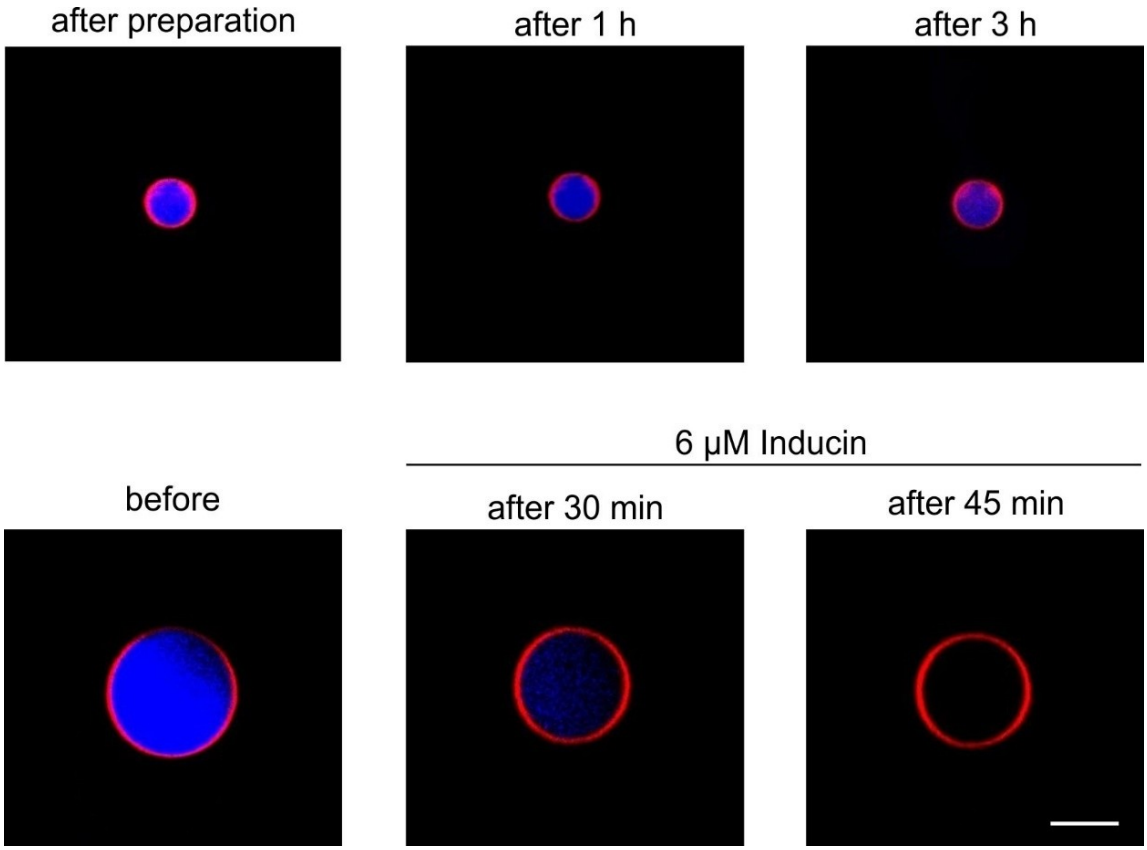

Figure 5. Influence of Inducin on membrane integrity. Confocal fluorescence microscopy snapshots (cross-sectional views) of POPC/POPG giant unilamellar vesicles at pH 7.4 before and after addition of 6 μM Inducin at the indicated time points and lipid-to-compound molar ratio of 10:1. To visualize the GUVs, the lipid bilayer was labeled with N–Rh-PE. At the same time, a water-soluble fluorophore, Atto 647, was entrapped inside the aqueous core surrounded by the lipid bilayer, serving as probe for membrane leakage. The size of Atto 647 is similar to that of the tested compounds. Scale bar: 10 μm.

Conclusions

LC3 lipidation occurs during canonical autophagy and is widely used as a marker of autophagosomes. However, LC3 is involved in cellular processes that go beyond autophagosome formation so detailed follow-up analysis is required to narrow down the trigger for LC3 lipidation. In a phenotypic assay monitoring LC3 puncta formation, we identified the Sinomenine-base pseudo-natural product termed Inducin that increases the number of LC3 puncta in the presence and absence of autophagy induction. The LC3 lipidation occurs independently of FIP200, the key component of the ULK1 complex that is essential for autophagy initiation, ruling out the involvement of canonical autophagy process. Instead, Inducin causes endolysosomal membrane damage resulting in the recruitment of the ESCRT machinery to lysosomes and activation of TFEB, which activates lysosomal biogenesis. Inducin disrupts lysosomal function, ultimately leading to cell death, most likely through lysosomal membrane permeabilization.

The cellular response to lysosome damage plays an important role in normal cell physiology, aging, and in pathogenic processes such as neurodegeneration and cancer. While a variety of physical, chemical and pathogenic agents have been shown to induce lysosomal damage in vivo, experimental models of damage have been mainly limited to the use of membranolytic peptides (LLOMe/GPN). It is likely that the cellular response to LMP will vary according to the nature of the damage, creating a need for additional small molecules capable of inducing LMP through alternative mechanisms. The Sinomenine-based pseudo-natural product Inducin represents a novel chemotype that induces LMP. Inducin accumulates in the lysosome and directly causes membrane damage. The mechanism for LMP induced by Inducin is different from that set in motion by LLOMe and GPN. In this regard, Inducin will be a valuable tool for broadening our understanding of the cellular response to LMP.

Experimental Section

Materials

Antibodies used in this study were from the following sources: LC3B (#2775, WB: 1:1000), FIP200 (#12436, WB: 1:1000), ATG12 (mouse specific) (#2011, WB: 1:1000), LAMP1 (#9091, IF: 1:200), and TFEB (#4240, WB: 1:1000) antibodies were purchased from Cell Signaling Technology. Anti-beta-actin antibody (A2228, WB: 1:10,000) was purchased from Sigma-Aldrich. p62/SQSTM1 (PM045, IF: 1:200) and LC3 (PM036, IF: 1:500) antibodies were purchased

from MBL international. ALIX (634502, IF: 1:200) antibody was purchased from BioLegend. Goat anti-rabbit-HRP (Cat# 31460, WB: 1:10,000) and goat anti-mouse-HRP (Cat# 31430, WB: 1:10,000) antibodies were purchased from Thermo Fisher. Alexa Fluor 488/568/647 conjugated secondary antibodies for immunofluorescence were purchased from Thermo Fisher. Leu-Leu methyl ester hydrobromide (LLOMe, L7393) was obtained from Sigma Aldrich. LysoTracker Red DND-99 (L7528) was obtained from Thermo Fisher.

Cell lines

MEFs (Atg5 +/+ and −/−: kind gift of Noboru Mizushima –Tokyo Medical and Dental University, Tokyo, Japan)[29] (FIP200 +/+ and −/−: kind gift of Jun-Lin Guan, University of Cincinnati, USA)[30] and HeLa cells (WT and mNeonGreen-TFEB: kind gift of Tamotsu Yoshimori, Osaka University, Japan)[4] were cultured in Dulbecco's modified Eagle medium (DMEM) (Sigma Aldrich) supplemented with 10% fetal bovine serum (FBS), penicillin/streptomycin, and non-essential amino acids at 37 °C with 5% CO_2. MCF7-GFP-LC3 were cultured in Minimum Essential Medium (Gibco) supplemented with 10% FBS (Sigma), 2 mM L-glutamine, 1 mM sodium pyruvate (Gibco) and 1% non-essential amino acids (Gibco) and 0,01 mg/ml insulin (Sigma). HeLa and U2OS cells were cultured in Dulbecco's Modified Eagle Medium (PAN biotech) supplemented with 10% FBS (Gibco), 1 mM sodium pyruvate (PAN biotech) and non-essential amino acids (PAN biotech). Cells were routinely tested for mycoplasma contamination using the LookOut mycoplasma PCR detection kit (Sigma Aldrich) or MycoAlert™ mycoplasma detection kit (Lonza).

Screening for LC3 puncta formation

MCF7-GFP-LC3 (4000 cells/ well) cells were seeded in 384 well plates (Greiner microclear). The next day cells were washed three times with 1x PBS using plate washer ELX405 (Agilent). After that, 10 μM of compound was added using Echo dispenser (Beckman Coulter) along with EBSS (starvation medium) and Chloroquine (50 μM) or medium containing Rapamycin (100 nM) and Chloroquine (50 μM). Three hours after incubation at 37 °C cells were fixed by addition of formaldehyde (4.6% final concentration) and simultaneously staining the nucleus with 1:500 Hoechst (Stock 1 mg/ml) for 20 min at RT. Fixed cells were washed thrice with 1× PBS using plate washer ELX405 (Agilent). For visualization of LC3 puncta, 4 pictures/well were acquired using ImageXpress Micro XL (Molecular Devices) at 20× magnification and analysed with the granularity algorithm of MetaXpress Software (Molecular Devices). Samples were normalized to DMSO treated cells. All calculations were done using Quattro Workflow software (Quattro Research GmbH).

Calculation of logP and bpKa values

Physicochemical properties (clogP, bpKa) were calculated from the SMILES representations of the structures using cxcalc, version 21.15.0, ChemAxon (http://www.chemaxon.com).

Phospholipidosis

Phospholipidosis was measured using the HCS LipidTOX™ Red reagent from Invitrogen according to the manufacturer's protocol. 3,000 U2OS cells were seeded in black 96-well plates with clear bottom and cultured overnight. Cells were than treated with the LipidTOX reagent and 2.5 μM Inducin or DMSO as a control (0.2%). Before formaldehyde fixation after 48 h treatment cells were incubated for 30 min in medium containing 5 μg/ml Hoechst-33342. Four images per well were acquired with the Zeiss Axiovert 200 M microscope using a 20x objective. Experiments were performed in quadruplicates and four images were taken per well.

LysoTracker Red DND-99 staining

Accumulation of lysosomotropic compounds in lysosomes was analyzed using the lysosomotropic fluorescent dye LysoTracker Red DND-99 (Invitrogen). U2OS cells were seeded in black clear-bottom 96-well plates at 7,000 cells/well and incubated overnight at 37 °C and 5% CO_2. The next day, the medium was replaced with medium containing compounds or 0.2% DMSO as a control. After 60 min incubation with the compounds at 37 °C and 5% CO_2, LysoTracker Red DND-99 and Hoechst-33342 were added to the medium at final concentrations of 1 μM and 1μg/ml, respectively, and cells were incubated for further 30 min at 37 °C and 5% CO_2. Cells were then fixed in 3.7% paraformaldehyde in PBS for 10 min at room temperature and washed thrice with PBS. Fluorescence imaging was performed using the Zeiss Axiovert 200 M microscope (Carl Zeiss, Germany). Four images per well were acquired using a 10x objective. The fluorescence intensity was analysed using CellProfiler image analysis software 4.2.1 (Carpenter et al., 2006). The LysoTracker Red DND-99 mean intensity per cell was calculated and normalized to the values of cells that were treated with DMSO.

Quantification and statistical analysis

All biological replicates were either representative of biological replicates or expressed as mean ± SD. All statistical details of the conducted experiments can be found in the respective figure and table legends. n: number of biological replicates.

General synthetic experimental details

All reactions were conducted open to air without precautions to exclude water unless specifically stated. Dry solvents were purchased from Fisher Scientific and/or Acros and used without further treatment. Thin layer chromatography (TLC) was performed on silica coated aluminium plates (Merck 60F254) and visualization was achieved under UV irradiation (254 nm). Purification of crude products was achieved through flash column chromatography (FC, silica gel 60, 0.035–0.070 mm) or automated medium pressure liquid chromatography (MPLC, Grace Reveleris X2) using the indicated solvents. In certain cases, 'magic mix' (50 DCM:8 EtOH:1 NH_4OH (50% aq.)) was used as a cosolvent for silica chromatography. Challenging separations were carried out on an Agilent 1100 preparative HPLC system equipped with a mass detector (columns: Nuleodur C18 gravity VP 125/10 5 μm, Nucleodur C18 gravity VP 125/21 5 μm, Nucleodur C4 gravity VP 125/10 5 μm). Appropriate gradient systems were applied by mixing water (+0.1% TFA) and either acetonitrile or methanol. NMR spectra were recorded on Bruker AV 400 Avance III HD (NanoBay), Agilent Technologies DD2, Bruker AV 500 Avance III HD (Prodigy), Bruker AV 600 Avance III HD (CryoProbe) or Bruker AV 700 Avance III HD (CryoProbe) spectrometers. Data is reported in ppm with reference to the used deuterated solvent.[31] High resolution mass spectrometry (HRMS) was performed on an LTQ Orbitrap mass spectrometer coupled to an Accela HPLC-System (HPLC column: Hypersyl GOLD, 50 mm x 1 mm, particle size 1.9 μm, ionization method: electron spray ionization (ESI)). Microwave reactions were carried out in a CEM Discover SP Activent machine.

Compounds **S1**, **2a**, **2b**, **3a–c**, **3e**, **3g–j**, **3o**, **3q–s**, **3aa–ae**, **4a–c**, **4e–4h**, **4m–4o**, **4q**, and **4r** were previously synthesized, and their

experimental details and spectra can be found in the corresponding publication.[10a] Compound S2 was synthesized following a literature procedure.[32]

Acknowledgements

Research at the Max Planck Institute of Molecular Physiology was supported by the Max Planck Society. Research at Umeå University was supported by the European Research Council (ChemBioAP), Vetenskapsrådet (Nr. 2018-04585, Nr. 2022-02932), the Knut and Alice Wallenberg Foundation and the Göran Gustafsson Foundation for Research in Natural Sciences and Medicine to Y.W.W. This work was co-funded by the European Union (Drug Discovery Hub Dortmund (DDHD), EFRE-0200481) and Innovative Medicines Initiative (grant agreement number 115489) resources of which are composed of financial contribution from the European Union's Seventh Framework Programme (FP7/2007-2013) and EFPIA companies' in-kind contribution. The compound management and screening center (COMAS) in Dortmund is acknowledged for performing the high-throughput screening. R.W. acknowledges funding by the Deutsche Forschungsgemeinschaft (DFG, German Research Foundation) under Germany's Excellence Strategy – EXC 2033 – 390677874 – RESOLV. We acknowledge the Biochemical Imaging Center at Umeå University and the National Microscopy Infrastructure, NMI (VR-RFI 2019–00217) for providing assistance in microscopy. Open Access funding enabled and organized by Projekt DEAL.

Conflict of Interests

The authors declare no competing interests.

Data Availability Statement

The data that support the findings of this study are available from the corresponding author upon reasonable request.

Keywords: biological activity · endolysosomal membrane damage · LC3 lipidation · lysosomal membrane permeabilization · small molecule

[1] D. J. Klionsky, A. K. Abdel-Aziz, S. Abdelfatah, M. Abdellatif, A. Abdoli, S. Abel, H. Abeliovich, M. H. Abildgaard, Y. P. Abudu, A. Acevedo-Arozena, I. E. Adamopoulos, K. Adeli, T. E. Adolph, A. Adornetto, E. Aflaki, G. Agam, A. Agarwal, B. B. Aggarwal, M. Agnello, P. Agostinis, J. N. Agrewala, A. Agrotis, P. V. Aguilar, S. T. Ahmad, Z. M. Ahmed, U. Ahumada-Castro, S. Aits, S. Aizawa, Y. Akkoc, T. Akoumianaki, H. A. Akpinar, A. M. Al-Abd, L. Al-Akra, A. Al-Gharaibeh, M. A. Alaoui-Jamali, S. Alberti, E. Alcocer-Gomez, C. Alessandri, M. Ali, M. A. Alim Al-Bari, S. Aliwaini, J. Alizadeh, E. Almacellas, A. Almasan, A. Alonso, G. D. Alonso, N. Altan-Bonnet, D. C. Altieri, E. M. C. Alvarez, S. Alves, C. Alves da Costa, M. M. Alzaharna, M. Amadio, C. Amantini, C. Amaral, S. Ambrosio, A. O. Amer, V. Ammanathan, Z. An, S. U. Andersen, S. A. Andrabi, M. Andrade-Silva, A. M. Andres, S. Angelini, D. Ann, U. C. Anozie, M. Y. Ansari, P. Antas, A. Antebi, Z. Anton, T. Anwar, L. Apetoh, N. Apostolova, T. Araki, Y. Araki, K. Arasaki, W. L. Araujo, J. Araya, C. Arden, M. A. Arevalo, S. Arguelles, E. Arias, J. Arikkath, H. Arimoto, A. R. Ariosa, D. Armstrong-James, L. Arnaune-Pelloquin, A. Aroca, D. S. Arroyo, I. Arsov, R. Artero, D. M. L. Asaro, M. Aschner, M. Ashrafizadeh, O. Ashur-Fabian, A. G. Atanasov, A. K. Au, P. Auberger, H. W. Auner, L. Aurelian, et al., *Autophagy* **2021**, *17*, 1.

[2] a) J. L. Nieto-Torres, A. M. Leidal, J. Debnath, M. Hansen, *Trends Biochem. Sci.* **2021**, *46*, 673; b) V. Deretic, M. Lazarou, *J. Cell Biol.* **2022**, *221*.

[3] E. Jacquin, S. Leclerc-Mercier, C. Judon, E. Blanchard, S. Fraitag, O. Florey, *Autophagy* **2017**, *13*, 854.

[4] S. Nakamura, S. Shigeyama, S. Minami, T. Shima, S. Akayama, T. Matsuda, A. Esposito, G. Napolitano, A. Kuma, T. Namba-Hamano, J. Nakamura, K. Yamamoto, M. Sasai, A. Tokumura, M. Miyamoto, Y. Oe, T. Fujita, S. Terawaki, A. Takahashi, M. Hamasaki, M. Yamamoto, Y. Okada, M. Komatsu, T. Nagai, Y. Takabatake, H. Xu, Y. Isaka, A. Ballabio, T. Yoshimori, *Nat. Cell Biol.* **2020**, *22*, 1252.

[5] R. Gomez-Sintes, M. D. Ledesma, P. Boya, *Ageing Res. Rev.* **2016**, *32*, 150.

[6] a) M. L. Skowyra, P. H. Schlesinger, T. V. Naismith, P. I. Hanson, *Science* **2018**, *360*; b) M. Radulovic, K. O. Schink, E. M. Wenzel, V. Nahse, A. Bongiovanni, F. Lafont, H. Stenmark, *EMBO J.* **2018**, *37*.

[7] F. Wang, R. Gomez-Sintes, P. Boya, *Traffic* **2018**, *19*, 918.

[8] D. L. Thiele, P. E. Lipsky, *Proc. Natl. Acad. Sci. USA* **1990**, *87*, 83.

[9] a) M. Grigalunas, S. Brakmann, H. Waldmann, *J. Am. Chem. Soc.* **2022**, *144*, 3314; b) G. Karageorgis, D. J. Foley, L. Laraia, H. Waldmann, *Nat. Chem.* **2020**, *12*, 227; c) G. Karageorgis, D. J. Foley, L. Laraia, S. Brakmann, H. Waldmann, *Angew. Chem. Int. Ed. Engl.* **2021**, *60*, 15705.

[10] a) M. Grigalunas, A. Burhop, S. Zinken, A. Pahl, J. M. Gally, N. Wild, Y. Mantel, S. Sievers, D. J. Foley, R. Scheel, C. Strohmann, A. P. Antonchick, H. Waldmann, *Nat. Commun.* **2021**, *12*, 1883; b) M. Akbarzadeh, J. Flegel, S. Patil, E. Shang, R. Narayan, M. Buchholzer, N. S. Kazemein Jasemi, M. Grigalunas, A. Krzyzanowski, D. Abegg, A. Shuster, M. Potowski, H. Karatas, G. Karageorgis, N. Mosaddeghzadeh, M. L. Zischinsky, C. Merten, C. Golz, L. Brieger, C. Strohmann, A. P. Antonchick, P. Janning, A. Adibekian, R. S. Goody, M. R. Ahmadian, S. Ziegler, H. Waldmann, *Angew. Chem. Int. Ed. Engl.* **2022**, *61*, e202115193; c) C. Davies, L. Dotsch, M. G. Ciulla, E. Hennes, K. Yoshida, R. Gasper, R. Scheel, S. Sievers, C. Strohmann, K. Kumar, S. Ziegler, H. Waldmann, *Angew. Chem. Int. Ed. Engl.* **2022**, *61*, e202209374; d) M. Grigalunas, S. Patil, A. Krzyzanowski, A. Pahl, J. Flegel, B. Scholermann, J. Xie, S. Sievers, S. Ziegler, H. Waldmann, *Chemistry* **2022**, *28*, e202202164; e) J. Liu, S. Mallick, Y. Xie, C. Grassin, B. Lucas, B. Scholermann, A. Pahl, R. Scheel, C. Strohmann, C. Protzel, T. Berg, C. Merten, S. Ziegler, H. Waldmann, *Angew. Chem. Int. Ed. Engl.* **2023**, e202301955.

[11] L. Galluzzi, D. R. Green, *Cell* **2019**, *177*, 1682.

[12] T. Hara, A. Takamura, C. Kishi, S. Iemura, T. Natsume, J. L. Guan, N. Mizushima, *J. Cell Biol.* **2008**, *181*, 497.

[13] a) O. Florey, S. E. Kim, C. P. Sandoval, C. M. Haynes, M. Overholtzer, *Nat. Cell Biol.* **2011**, *13*, 1335; b) J. Martinez, R. K. Malireddi, Q. Lu, L. D. Cunha, S. Pelletier, S. Gingras, R. Orchard, J. L. Guan, H. Tan, J. Peng, T. D. Kanneganti, H. W. Virgin, D. R. Green, *Nat. Cell Biol.* **2015**, *17*, 893.

[14] a) S. Chauhan, S. Kumar, A. Jain, M. Ponpuak, M. H. Mudd, T. Kimura, S. W. Choi, R. Peters, M. Mandell, J. A. Bruun, T. Johansen, V. Deretic, *Dev. Cell* **2016**, *39*, 13; b) I. Maejima, A. Takahashi, H. Omori, T. Kimura, Y. Takabatake, T. Saitoh, A. Yamamoto, M. Hamasaki, T. Noda, Y. Isaka, T. Yoshimori, *EMBO J.* **2013**, *32*, 2336.

[15] a) S. Aits, J. Kricker, B. Liu, A. M. Ellegaard, S. Hämälistö, S. Tvingsholm, E. Corcelle-Termeau, S. Høgh, T. Farkas, A. Holm Jonassen, I. Gromova, M. Mortensen, M. Jäättelä, *Autophagy* **2015**, *11*, 1408; b) I. Paz, M. Sachse, N. Dupont, J. Mounier, C. Cederfur, J. Enninga, H. Leffler, F. Poirier, M. C. Prevost, F. Lafont, P. Sansonetti, *Cell. Microbiol.* **2010**, *12*, 530.

[16] J. Jia, A. Claude-Taupin, Y. Gu, S. W. Choi, R. Peters, B. Bissa, M. H. Mudd, L. Allers, S. Pallikkuth, K. A. Lidke, M. Salemi, B. Phinney, M. Mari, F. Reggiori, V. Deretic, *Dev. Cell* **2020**, *52*, 69.

[17] M. Radulovic, K. O. Schink, E. M. Wenzel, V. Nähse, A. Bongiovanni, F. Lafont, H. Stenmark, *EMBO J.* **2018**, *37*.

[18] J. Jia, Y. P. Abudu, A. Claude-Taupin, Y. Gu, S. Kumar, S. W. Choi, R. Peters, M. H. Mudd, L. Allers, M. Salemi, B. Phinney, T. Johansen, V. Deretic, *Mol. Cell* **2018**, *70*, 120.

[19] R. Puertollano, S. M. Ferguson, J. Brugarolas, A. Ballabio, *EMBO J.* **2018**, *37*.

[20] Y. Xu, P. Zhou, S. Cheng, Q. Lu, K. Nowak, A. K. Hopp, L. Li, X. Shi, Z. Zhou, W. Gao, D. Li, H. He, X. Liu, J. Ding, M. O. Hottiger, F. Shao, *Cell* **2019**, *178*, 552.

[21] O. Florey, N. Gammoh, S. E. Kim, X. Jiang, M. Overholtzer, *Autophagy* **2015**, *11*, 88.

[22] a) T. Yoshimori, A. Yamamoto, Y. Moriyama, M. Futai, Y. Tashiro, *J. Biol. Chem.* **1991**, *266*, 17707; b) K. Niikura, *Drug News Perspect.* **2006**, *19*, 139.
[23] O. F. Kuzu, M. Toprak, M. A. Noory, G. P. Robertson, *Pharmacol. Res.* **2017**, *117*, 177.
[24] S. Nadanaciva, S. Lu, D. F. Gebhard, B. A. Jessen, W. D. Pennie, Y. Will, *Toxicol. in Vitro* In Vitro **2011**, *25*, 715.
[25] B. Breiden, K. Sandhoff, *Biol. Chem.* **2019**, *401*, 31.
[26] a) N. Kavcic, K. Pegan, B. Turk, *Biol. Chem.* **2017**, *398*, 289; b) A. C. Johansson, H. Steen, K. Ollinger, K. Roberg, *Cell Death Differ.* **2003**, *10*, 1253.
[27] J. R. Lakowicz, Springer New York, NY **2006**, Ed. 3.
[28] D. Casares, P. V. Escriba, C. A. Rossello, *Int. J. Mol. Sci.* **2019**, *20*.
[29] A. Kuma, M. Hatano, M. Matsui, A. Yamamoto, H. Nakaya, T. Yoshimori, Y. Ohsumi, T. Tokuhisa, N. Mizushima, *Nature* **2004**, *432*, 1032.
[30] B. Y. Gan, X. Peng, T. Nagy, A. Alcaraz, H. Gu, J. L. Guan, *J. Cell Biol.* **2006**, *175*, 121.
[31] G. R. Fulmer, A. J. M. Miller, N. H. Sherden, H. E. Gottlieb, A. Nudelman, B. M. Stoltz, J. E. Bercaw, K. I. Goldberg, *Organometallics* **2010**, *29*, 2176.
[32] A. Kimishima, C. J. Wenthur, B. Zhou, K. D. Janda, *ACS Chem. Biol.* **2017**, *12*, 36.

Manuscript received: August 17, 2023
Revised manuscript received: October 16, 2023
Accepted manuscript online: October 23, 2023
Version of record online: November 7, 2023